Quasiparticle scattering in 3 MeV proton irradiated $BaFe_2(As_{0.67}P_{0.33})_2$

Akiyoshi Park, Sunseng Pyon, Yue Sun, Ivan Veshchunov, Jingting Chen, Nozomu Ito, Takahiro Suwa, and Tsuyoshi Tamegai
Department of Applied Physics, The University of Tokyo, Hongo, Bunkyo-ku, Tokyo 113-8656, Japan

Hisashi Kitamura
National Institute of Radiological Sciences, National Institutes for Quantum and Radiological Science and Technology, Anagawa, Chiba-shi, Chiba 263-8555, Japan

Ataru Ichinose
Central Research Institute of Electric Power Industry, Electric Power Engineering Research Laboratory, 2-6-1 Nagasaka, Yokosuka-shi, Kanagawa 240-0196, Japan

(Received 25 June 2017; revised manuscript received 29 July 2018; published 20 August 2018)

Effects of 3 MeV H^+ (proton) irradiation on superconductivity in $BaFe_2(As_{0.67}P_{0.33})_2$ was investigated through *in situ* resistivity measurements and magnetotransport measurements. The suppression of T_c by H^+ irradiation is more moderate in comparison with electron irradiation, yet more effective than that of irradiation of heavier He^+ ions. Surprisingly, the B-linear magnetoresistance (MR) in the pristine crystal crosses over to an anomalous negative MR after the irradiation. We discuss that the negative MR is most likely to emanate from sparse magnetic impurities. The appearance of a paramagnetic signal in magnetization measurements supports the existence of magnetic impurities in the sample. Although the estimated concentration of local magnetic moments suggests that the concentration of magnetic impurities is dilute, thereby signifying that irradiation-induced defects are dominantly nonmagnetic, the role of magnetic scattering cannot be completely neglected. Hence, H^+ irradiation in this system contains magnetic-scattering centers, which are pair breakers for both the s_{++}- and the $s_{\pm}$-gap structures, indicating that the suppression of T_c is a consequence of both magnetic and nonmagnetic scatterings. This result opens up the possibility for the scenario of the slow but steady suppression of T_c emanating from the s_{++}-gap symmetry with pair breaking due to dilute magnetic scatterers.

DOI: 10.1103/PhysRevB.98.054512

I. INTRODUCTION

Disorder is a powerful phase-sensitive utility in allowing one to probe the pairing interaction in superconductors. As asserted in Anderson's theorem, in conventional isotropic s-wave superconductors, nonmagnetic-scattering centers in the weak disorder regime bear no impact on the superconducting transition temperature (T_c) [1]. On the other hand, perturbations that break time-reversal symmetry induced, for example, by magnetic impurity scattering produce midgap bound states, impairing superconductivity in accordance with the Abrikosov-Gor'kov (AG) equation [2]. An extension of this rudimentary theory is applied to superconductors with unconventional gap structures where nonmagnetic impurities in those with symmetry-protected gaps, such as the d-wave or $s_{\pm}$-wave gap symmetry scatter quasiparticles between sign-reversing gaps. Such a scenario leading to the formation of midgap states suppresses T_c following the AG framework [3,4].

Albeit recent experimental investigations strongly advocating the sign-reversing $s_{\pm}$-gap structure in iron-based superconductors (IBSs), experimental investigations through chemical doping and light-particle irradiation indicate a suppression of T_c with increasing nonmagnetic impurities much slower than that of the AG theory [5–8]. The inconsistency of the slow T_c suppression rate is currently rationalized through two competing theories: (1) A scenario of the sign-preserving s_{++} gap without impurity-induced midgap states thereby being insensitive to scattering [9,10], and (2) a scenario of the $s_{\pm}$ gap with a realistic finite-ranged impurity potential [$U^{\rm imp}(\mathbf{q})$] with a stronger intraband than the interband scattering potential ($U^{\rm imp}_{\rm intra} > U^{\rm imp}_{\rm inter}$), which results in a passive T_c suppression [11]. Experimentally, the T_c suppression by electron irradiation on isovalently substituted $Ba(Fe_{0.76}Ru_{0.24})_2As_2$ has been claimed to be consistent with a two-band $s_{\pm}$-gap scenario with variable scattering potential strength thereby ruling out the likelihood of the s_{++}-gap case [12]. This claim is further supported by the argument that electron irradiation results in a T_c suppression rate closer to the AG model as it induces true lattice interstitial/vacancy, closer to the ideal strong pointlike scatterers ($U^{\rm imp}_{\rm intra} = U^{\rm imp}_{\rm inter}$) in contrast to proton (H^+) irradiation which is assumed to create larger clustered defects. Yet, the scattering properties of experimentally induced impurities lack a clear understanding.

To deconvolute discussions on the effect of impurities on superconductivity, it is therefore crucial to identify the characteristics of the artificially incorporated defects and the scattering properties they devise. In this paper, we employ $BaFe_2(As_{0.67}P_{0.33})_2$, a prototypical IBS with isovalent doping, subject to 3 MeV H^+ irradiation. Extensive studies on the material have proclaimed that optimal doping coincides with the quantum critical point, notably by exhibiting

non-Fermi-liquid linear temperature dependence of resistivity through a wide range of temperatures [13], despite the still on-going debate [14,15]. Analogous to the empirical T-linear relationship $\hbar/\tau = \alpha k_B T$, a B-linear relationship $\hbar/\tau = \beta \mu_B B$ has been reported, where α and β are proportionality constants on the order of unity, implying that temperature and magnetic fields are both dominant energy scales that determine the scattering rate of quasiparticles in this particular system [16]. Although such phenomena were realized in $BaFe_2(As_{0.67}P_{0.33})_2$, which resides in the clean limit, whether adding on to the quasiparticle scattering through engineering defects into the system would modify the temperature and field dependences remains obscure.

In light of this, the objective of this investigation is to attempt to suppress superconductivity through the incorporation of scattering centers through H^+ irradiation in $BaFe_2(As_{0.67}P_{0.33})_2$ and examine its effect on: (1) T_c and (2) on the scattering rate at varying temperatures and magnetic fields, hence, gaining insight into the effects of disorder on transport and superconductivity in IBSs.

II. EXPERIMENT: CRYSTAL GROWTH AND IRRADIATION

$BaFe_2(As_{0.67}P_{0.33})_2$ single crystals were grown through a Ba_2As_3/Ba_2P_3 flux method [17]. Presynthesized Ba_2As_3, Ba_2P_3, FeAs, and FeP were placed in an alumina crucible and vacuum sealed in a quartz tube. All procedures were carried out in a glovebox with a N_2 atmosphere in order to prevent oxidation of chemically unstable Ba_2As_3 and Ba_2P_3. The assembly was heated to 1150 °C and cooled to 900 °C over a period of 250 h in an electric furnace, yielding crystals of several millimeters. The chemical stoichiometry was determined through both energy dispersive x-ray analysis and the angle of the (008) peaks in the x-ray diffraction pattern. The superconducting transition temperature T_c was determined by the onset of the diamagnetic response showing that $T_c = 29.4$ K with a sharp transition width of $\Delta T_c \approx 1$ K, indicating the high quality and the high homogeneity of the crystal. In order to ensure that the crystals are identical in character, the samples subject to measurements were collected from the same batch.

The crystals obtained were cleaved into a thickness of < 30 μm to allow for homogeneous incorporation of defects through H^+ irradiation. In order to monitor the effect of irradiation on the scattering rate and T_c, the resistivity was measured *in situ*. The advantage of an *in situ* approach is that the sample subject to irradiation can be maintained at low temperatures of less than 50 K, preventing room-temperature annealing of irradiation-induced defects. The resistivity was measured through a four-terminal method with gold pads sputtered on the surface in order to reduce contact resistance. On the gold pads, 25 μm diameter gold wires were attached using silver paste. Here, two samples were subjects for irradiation, denoted as No. 1 and No. 2 hereafter. To prevent overheating of the crystal, the H^+ flux was bound under 10^{12} ions cm^{-2} s^{-1}, and resistivity measurements were performed at least 30 min after the irradiation to ensure the sample was at thermal equilibrium.

The crystals were mounted on a sapphire plate and irradiated along the c axis at the National Institute of Radiological Sciences Heavy Ion Medical Accelerator in Chiba at 50 K with a ^{4}He refrigerator. After the *in situ* resistivity measurements were completed, the samples were heated to room temperature. Without disturbing the electrical contacts on the crystal, magnetoresistance was measured using a physical property measurement system (Quantum Design) with a four-probe ac lock-in method.

III. RESULTS

A. *In situ* resistivity measurements

As shown in Figs. 1(a) and 1(b), the pristine transition temperature (T_{c0}) of No. 1 and No. 2 prior to irradiation are 29.5 and 28.6 K in the respective order; the transition temperatures were quantified as the midpoint of the transition. The slight resistive upturn in No. 2 stems from the antiferromagnetic phase residing in the slightly underdoped region. After the irradiation, both samples experience a drop in the T_c and

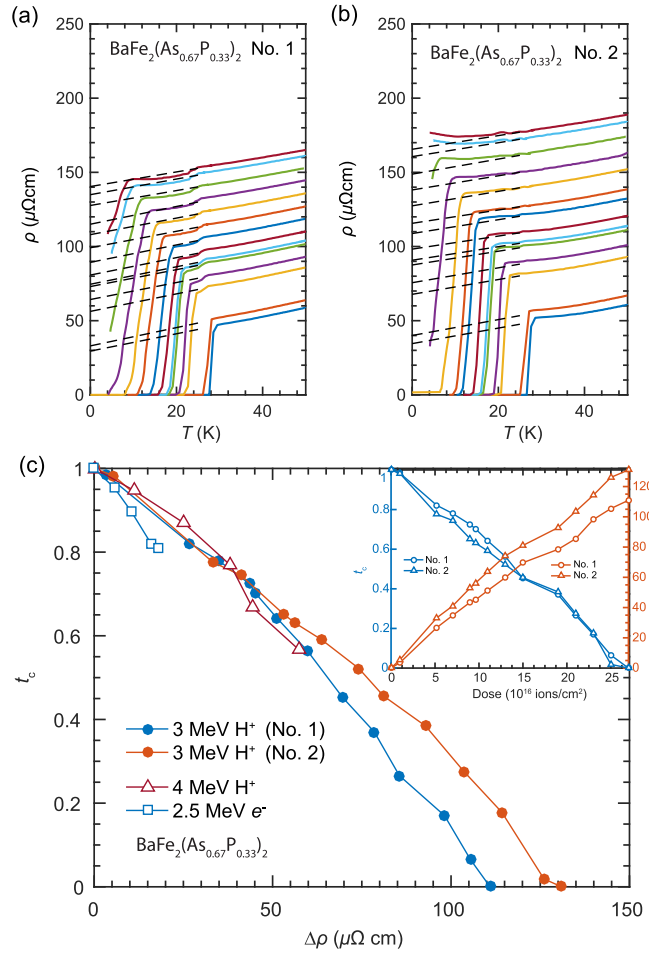

FIG. 1. (a) and (b) Temperature dependence of resistivity with an increasing H^+ dose below 50 K of two $BaFe_2(As_{0.67}P_{0.33})_2$ crystals, No. 1 and No. 2. (c) Comparison of T_c suppression in this paper with 2.5 MeV electron irradiation [18] and 4 MeV H^+ irradiation [19], depicted by $\Delta\rho$ versus t_c. The inset indicates the dose dependence of $\Delta\rho$ and t_c of $BaFe_2(As_{0.67}P_{0.33})_2$ No. 1 and No. 2 revealed through this investigation.

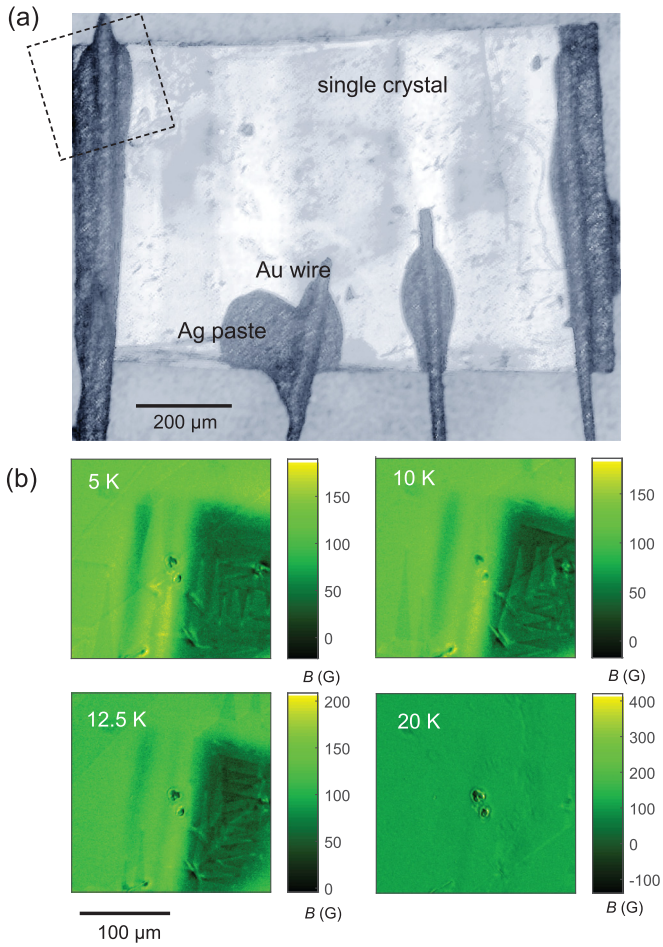

FIG. 2. (a) Optical microscope image of $BaFe_2(As_{0.67}P_{0.33})_2$ No. 1 with the electric contacts attached to the crystal surface. The outer two contacts are connected to a current source, and the inner two contacts are attached to a digital voltmeter. Moreover, the area enclosed in the dotted lines indicates the section subject to magneto-optical (MO) imaging. (b) MO image of No. 1 at various temperatures in a field of 100 Oe parallel to the crystal *c* axis after zero-field cooling.

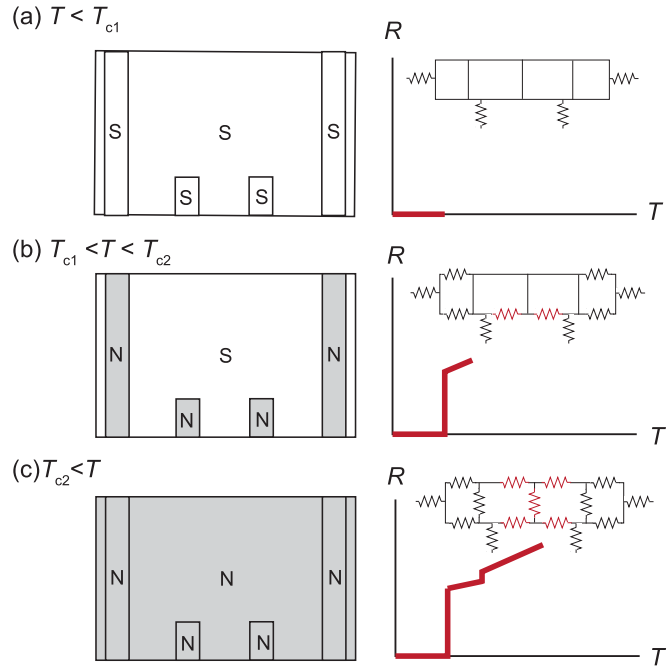

FIG. 3. A scheme of the planar view of the sample surface at various temperatures is shown on the left. Here, "*S*" represents the region in the superconducting state, and "*N*" represents the region of the normal state. The corresponding temperature dependence of resistivity at various temperatures is shown on the right. The inset represents the equivalent circuit of the sample.

increase in the scattering rate, suggesting that defects prompted by the irradiation are effective pair breakers.

Not to mention, for both No. 1 and No. 2, an anomalous structure in the temperature dependence of resistivity is observed between T_c and T_{c0}. Such a structure appearing right above T_c is a consequence of the experimental setup employed for *in situ* resistivity measurements. Ideally, particle irradiation on the sample should be homogeneous. However, due to interference caused by the electrical contacts attached to the surface of the crystal, the region of the sample beneath the contacts [Fig. 2(a)] is irradiated by particles with lower energy. In order to understand the effects of irradiation underneath the contacts, MO imaging of a section of the irradiated sample was observed. As exhibited in Fig. 2(b), superconductivity in the region underneath the contacts is strongly suppressed; in other words, it has a relatively lower T_c than the surrounding region. This is because the contacts on top of the crystal cause energy decay of the irradiated particle, thereby increasing the energy deposition per distance traveled, destroying a larger portion of the crystal. Thus, the crystal consists of a region with low T_c (T_{c1}) and high T_c (T_{c2}). At temperatures well below T_{c1}, superconductivity is maintained throughout the whole sample [Fig. 3(a)]. However, for $T_{c1} < T < T_{c2}$, normal regions underneath the contacts appear, contributing to finite resistance [Fig. 3(b)]. Above T_{c2}, the whole superconductor transitions to the normal state [Fig. 3(c)]. Such two-step temperature dependence explicates the structure in the vicinity of the temperature dependences of resistivity in the irradiated sample.

To make quantitative discussions on the impurity scattering rate, the zero-temperature resistivity (ρ_0) was extrapolated through fitting the resistance above T_c to the following linear function: $\rho = \rho_0 + AT$. The temperature dependences of resistivity are aligned parallel to each other with the coefficient $A \approx 0.5\ \mu\Omega\,\mathrm{cm\,K^{-1}}$ after each dose, which surprisingly is in stark contrast to that of Ref. [19] where a greater temperature dependence is observed after H^+ irradiation. The nonchanging slope of the temperature dependence of resistivity with an increasing H^+ dose even after superconductivity is fully suppressed, signifies the robustness of the energy scale in determining the T-linear scattering in the quantum critical point. Using ρ_0, the evolution of the resistivity was obtained through $\Delta\rho = \rho_0^i - \rho_0^0$, where the superscript i represents the ith irradiation resistivity and the T_c suppression was obtained with ($\Delta T_c = T_{c0} - T_c$). Moreover, the average $\Delta T_c/\Delta\rho$ was quantified through the slope determined by linear regression analysis of the ΔT_c versus $\Delta\rho$ plot in the range of $0.8 < t_c(= T_c/T_{c0}) < 1$ [Fig. 1(c)]. In this experiment, $\Delta T_c/\Delta\rho$ is -0.25 and $-0.20\ \mathrm{K}\,\mu\Omega^{-1}\,\mathrm{cm}^{-1}$ for No. 1 and No. 2, respectively, which is comparable to the suppression rate for the 4 MeV

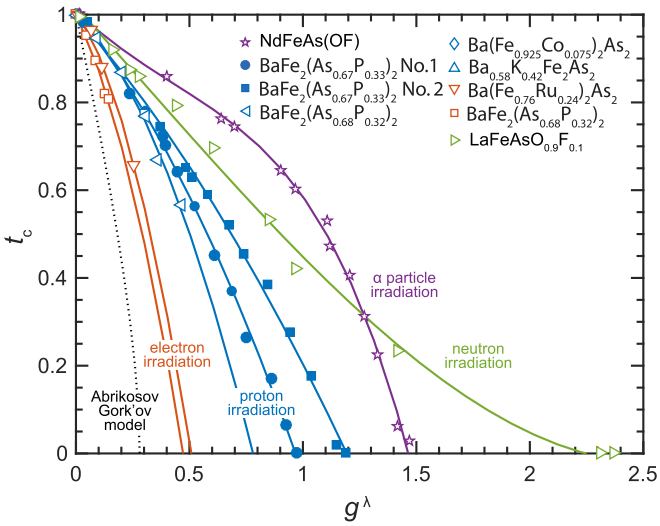

FIG. 4. Dimensionless scattering rate g^λ of e^-, neutron, H^+, and He^+ particle irradiations on various types of IBSs compared with that proposed by the AG theory [18–21].

H^+ irradiation experiment of -0.15 K $\mu\Omega^{-1}$ cm^{-1} [19], yet slower than electron irradiation showing -0.33 K $\mu\Omega^{-1}$ cm^{-1} [18]. It is noteworthy that, in this investigation, we were able to heavily irradiate the samples to an extent where superconductivity is fully destroyed and recognize that rather than exhibiting a linear ρ_0 versus ΔT_c, the suppression rate steepens at higher irradiation doses as observed in Ref. [19].

For further discussions, the normalized impurity scattering rate (g) is estimated from the Drude model,

$$g = \frac{\hbar}{2\pi k_B T_{c0}\tau} = \frac{\hbar n e^2 \Delta\rho}{2\pi k_B T_{c0} m^*}, \quad (1)$$

where τ is the quasiparticle scattering time, n is the carrier density, and m^* is the effective mass of the quasiparticle. The penetration depth $\lambda_0 = \sqrt{m^*/\mu_0 n e^2}$ is used to quantify τ such that g can be calculated solely from λ,

$$g^\lambda = \frac{\hbar \Delta\rho}{2\pi k_B T_{c0} \mu_0 \lambda_0^2}. \quad (2)$$

Using the penetration depth $\lambda_0 = 200$ nm evaluated from a tunnel diode oscillator experiment for $BaFe_2(As_{0.67}P_{0.33})_2$ [22], g^λ was plotted against the corresponding t_c. As depicted in Fig. 4, the normalized scattering rate intercepts the $t = 0$ axis at $g^{crit} \approx 1.0$, whereas the suppression rate described by the Abrikosov-Gork'ov theory,

$$-\ln(t_c) = \psi\left(\frac{1}{2} + \frac{g}{2t_c}\right) - \psi\left(\frac{1}{2}\right), \quad (3)$$

where ψ is the digamma function predicts a critical value of $g^{crit} \approx 0.3$. Moreover, T_c suppression emanating from electron irradiation indicates a critical value more consistent with that of the AG model with approximately $g^{crit} \approx 0.5$ [12,18]. It should be noted that α-particle irradiation in NdFeAs(O,F) suppresses T_c with a significantly slower rate with $g^{crit} \approx 1.5$ [20]. An even slower T_c suppression is evident in neutron-irradiated $LaFeAsO_{0.9}F_{0.1}$ [21].

These trends are common for a wide range of IBSs, indicating that rather than the intrinsic properties of the irradiated material, the type of damage caused by the irradiated particles heavily influences the suppression of T_c.

B. Defect morphology

To elucidate the deviation from the ideal strong pointlike scattering situation ($U^{imp}_{intra} = U^{imp}_{inter}$), the cross section of the sample was subject to scanning transmission electron microscopy (STEM) to directly observe the size and morphology of the defects in the irradiated crystal. Numerical calculations have reported that H^+ irradiation creates cascades and clusters of point defects in the crystal, much larger than atomic interstitials and vacancies [18,19]. Although direct observations have never been reported, understanding the size and the shape of the defect generated through the process of irradiation is critical in gaining knowledge of the scattering mechanism.

The sample subject to STEM imaging was irradiated up to a total dose of 27×10^{16} ions/cm^2 [the final irradiation dose $T_c < 4.2$ K (the minimum temperature reached in the ^{4}He refrigerator)], then was cut using a focused ion beam to reveal the cross-sectional plane, taken on the approximate midpoint between the top surface and the bottom surface of the crystal. The cross-sectional STEM image of the H^+ irradiated sample [Fig. 5(b)] exhibits black speckles much stronger than those in the pristine sample [Fig. 5(a)]. From the fact that the strong speckles are only present in the irradiated samples, we rationalize that they are related to defects in the crystal derived from irradiation. Each of the defects typically has a radius of up to $\approx$5 nm as revealed in Fig. 5, which is comparable to the coherence length of $\xi_0 = 1.6$ nm [23]. For further analysis, the degree of disorder in the crystal generated from irradiation was quantified through geometrical phase analysis (GPA) of TEM images [Figs. 6(c) and 6(d)]. TEM images were analyzed over STEM images to keep out any phase distortion caused by scan noise. The degree of strain, just by sight, is larger in the irradiated sample than in the pristine sample. Each of the highly strained domains is of nanometer scale. Even from the histogram of Fig. 6(e), which shows the distribution of in-plane strain ε_{xx}, averaged from four TEM images, it becomes clear that there is a larger number of areas with a high degree of ε_{xx}, indicative of an increase in the degree of disorder in the crystal after irradiation.

Therefore, rather than each of the atomic-scale defects being homogeneously distributed within the crystal, defects are distributed to form nanoscale clusters with highly distributed radii. In contrast to ideal point scatterers with uniform atomic size, the varying defect sizes in this experiment imply that the scattering centers encompass a wide range of scattering lengths. In particular, long-range scatterers span wave vectors in k space within bands thereby mainly contributing to intraband scattering. As intraband scattering does not contribute to pair-breaking T_c [24], the observed defects here are consistent with the slow T_c suppression rate. Yet, undoubtedly, the effect of H^+ irradiation is in stark contrast to the effects of heavy-ion irradiation, such as in Au, Pb, and U which create linear tracks of columnar defects [Fig. 5(c)] [25,26].

Moreover, in contrast to 190 keV H^+ irradiation which generates cascade-type defects, STEM images reveal that

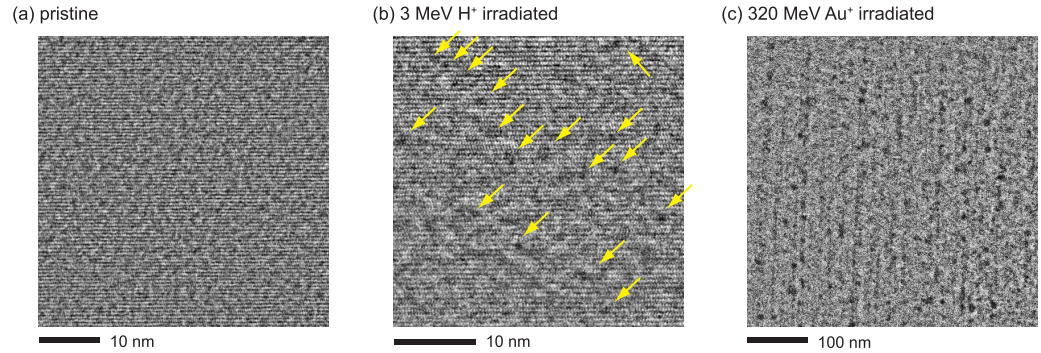

FIG. 5. Cross sections of $BaFe_2(As_{0.67}P_{0.33})_2$ observed through STEM. Here, the cross-sectional images shown are (a) pristine, (b) 3 MeV H^+ irradiated in which the yellow arrows indicate the defects, and (c) 320 MeV Au^+ irradiated. The horizontal stripes in the STEM images indicate the FeAs layers.

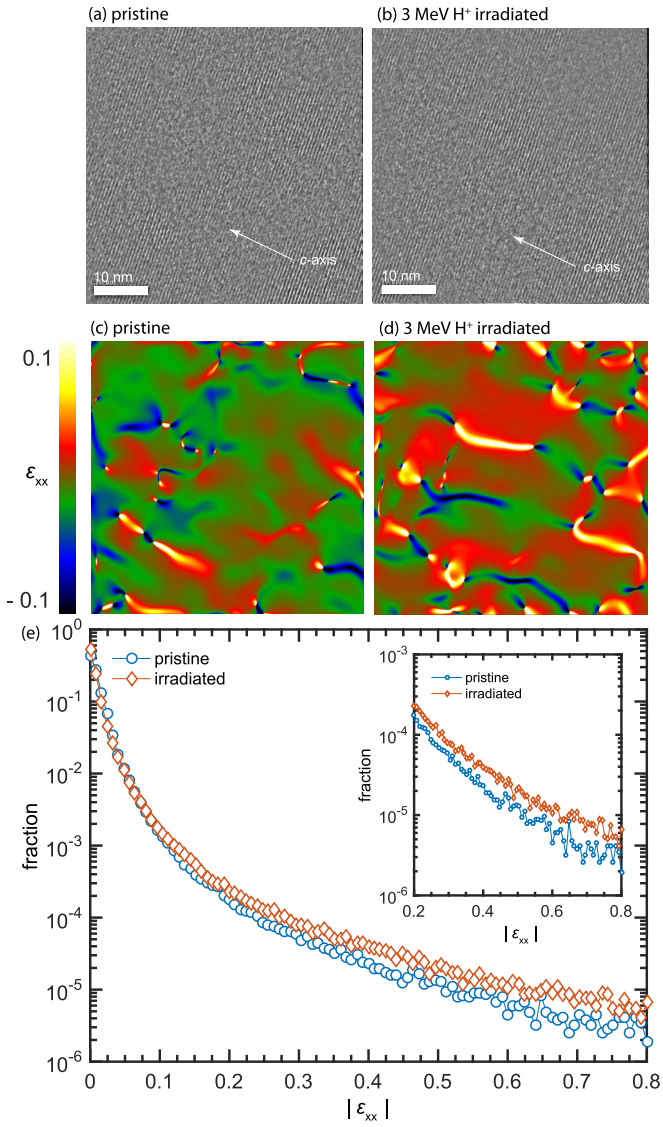

FIG. 6. Cross-sectional TEM images of (a) the pristine, (b) the irradiated sample, (c) and (d) the strain map of in-plane ε_{xx} determined through GPA. (e) A histogram of ε_{xx} averaged from four TEM images. The inset is a blowup of the range of $\varepsilon_{xx} \approx 0.2$–$0.8$ to emphasize the increase in strain in the irradiated sample.

irradiation of higher energies as in this paper results in defects of a more pointlike nature [27]. The key difference between the two types of irradiation is the relationship between the location the peak of the Bragg curve and the sample thickness. For the case of Ref. [27] in which cascade-type defects were observed, the Bragg peak is located at 100 nm, around the same length of the sample thickness of $\approx$ 100–130 nm. On the other hand, the 3 MeV H^+, the Bragg peak, which is approximately 57 μm as revealed from stopping and the range of the ions in the matter calculations [28], is much longer than the sample thickness of 10 μm, bringing about minimal energy deposition per path traveled with small recoil, contributing to mainly point defects. It is noteworthy that, since the samples were exposed to room temperature for STEM imaging, the sample was accountable for room-temperature annealing, which destabilizes and eliminates defects to a certain extent.

C. Magnetoresistance measurements

Once the irradiation was complete, the samples were exposed to room temperature for 6 weeks, stored in a vacuum desiccator, and then studied for their magnetotransport properties. After being exposed to room temperature, the irradiated samples experienced a sharpening in the resistivity drop with a shift of onset T_c to a higher temperature (Fig. 7).

As exhibited in the magnetoresistance (MR) at various temperatures illustrated in Fig. 8 below T_c, a sharp increase in resistivity is recognized due to flux flow resistivity in the superconducting phase [29]. At 30 K, slightly above T_c, a H-linear MR is observed in a wide range of fields. Furthermore, above T_c in the normal state, the resistivity follows a conventional quadratic relationship $\propto H^2$ at lower fields [30], whereas it crosses over to a linear MR at even higher fields due to the presence of spin-density wave order [31]. It has been reported that, at even higher fields of up to 92 T, the linearity is maintained with scalability between magnetic field and temperature, implying that the high-field H-linear behavior could have the same origin as the T-linear behavior characteristic of the quantum critical point [16,32]. However, as shown in the MR of highly disordered $BaFe_2(As_{0.67}P_{0.33})_2$(No. 1) in which $t_c = 0.3$, such linearity seen in the pristine sample collapses (Fig. 9). As the temperature is further increased, the MR at higher fields saturates and surprisingly shows a negative quadratic field dependence above T_{c0} [Figs. 9(i) and 9(j)].

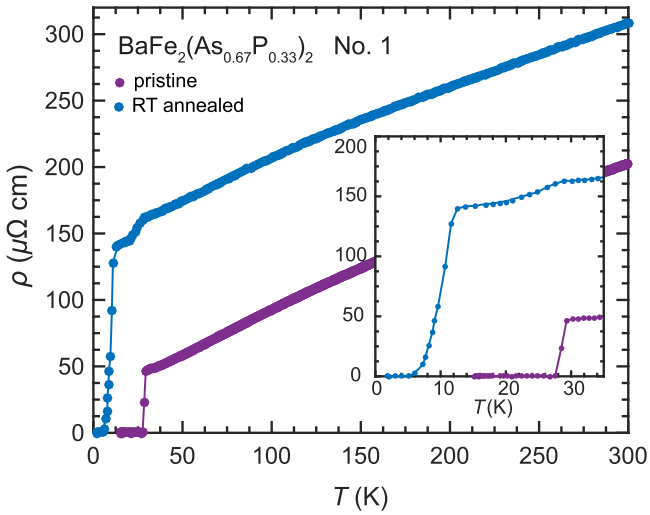

FIG. 7. The effect of room-temperature annealing depicted by the temperature dependence of resistivity before the irradiation and 6 weeks after irradiation being exposed to room temperature. The inset shows the blowup between 0 and 35 K.

It is clearly important to rationalize such anomalous negative MR observed in the disordered sample. For macroscopic samples, a negative MR among disordered systems can be accounted for by several different phenomena.

(I) One is the kinetic interference phenomena of electrons in the variable-range hopping conduction regime [33]. However, this scenario does not seem to fit the present case as hopping conduction occurs between localized electronic states of the system that reside in the critical regime of the metal-insulator transition. Moreover, localized states are not compatible with the periodicity of the crystal structures [34].

(II) The second possible origin of the anomalous MR is the notion that disorder brings about spatial fluctuations in the superconducting order parameter, ultimately resulting in numerous superconducting islands [35,36]. Since the magnetic field decreases the size of the superconducting islands thus increasing its charging energy, electron transport via the normal "sea" surrounding the islands becomes favorable and more dominant. A further increase in the magnetic field decreases the size of the islands and increases the number of paths available for electron transport, hence, reducing resistance. Such a picture depicts cases in the vicinity of the percolation limit. Importantly, the depicted negative MR mechanism can only occur with the coexistence of the superconducting phase and normal phase, in other words, limited to temperatures below T_c. However, the negative MR is revealed only above T_c thereby not being applicable to the current case.

(III) This leaves us with the most feasible explanation for the negative MR: the contribution of magnetic scattering induced by the defects. When the irradiated particle collides with an atom in the target crystal, ions in the crystal are dislocated. The irradiated particles, in particular, affects the spin state of the dislocated Fe ion; whereas the local magnetic moment of Fe in $BaFe_2As_2$ has a total magnetic moment of $\mu_s = 1.3\mu_B$, the magnetic moment of a free Fe^{2+} is $4.9\mu_B$ [37]. Intuitively, irradiation would therefore allow for a congregation of both magnetic- (Fe^{2+} and Fe^{3+} interstitials) and nonmagnetic- (vacancies) scattering centers.

The presence of magnetic impurities can give rise to spin-dependent scattering. When the electron spin and the magnetic field of the impurity are parallel, the probability of electron scattering decreases, whereas the resistance increases when the two are antiparallel [38]. Through applying a uniform external magnetic field, scattering of different spin-dependent processes could be suppressed thereby resulting in a negative MR. There have been previous reports on 200 keV α-particle- (He^+-) irradiated $Ba(Fe_{1-x}Co_xAs)_2$ thin films exhibiting crossover from positive to negative magnetoresistance for temperatures above $T_{c0} = 24.5$ K [39] and in neutron-irradiated polycrystalline $LaFeAsO_{0.9}F_{0.1}$ [21]. Although the lack of the logarithmic upturn in the temperature dependence of resistivity due to the Kondo effect suggests the small effect of magnetic scattering, a method with a considerable resolution must be used to quantify the effect of magnetic-scattering centers in the system.

D. Magnetic susceptibility measurements

To directly reveal the existence of such magnetic impurities, the sample was subject to magnetization measurements. Figure 10 exhibits the temperature dependence of magnetization field cooled from 150 to 2 K under a field of 10 kOe. Here, the molar susceptibility was calculated from the volume of the chemical formula unit 99 $Å^3$, which is half the value of the unit-cell volume of 199 $Å^3$ [40]. The irradiated sample

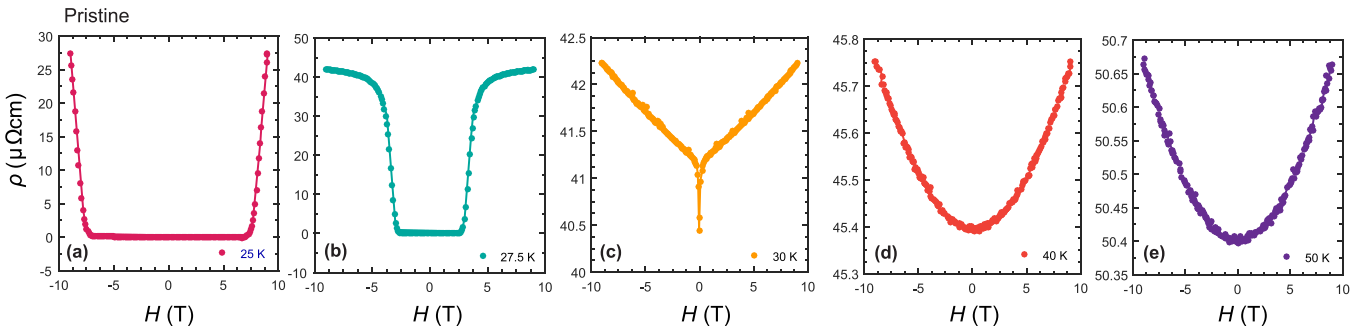

FIG. 8. The magnetoresistance of pristine $BaFe_2(As_{0.67}P_{0.33})_2$ No. 1 between −9 and 9 T at temperatures of (a) 25 K, (b) 27.5 K, (c) 30 K, (d) 40 K, and (e) 50 K.

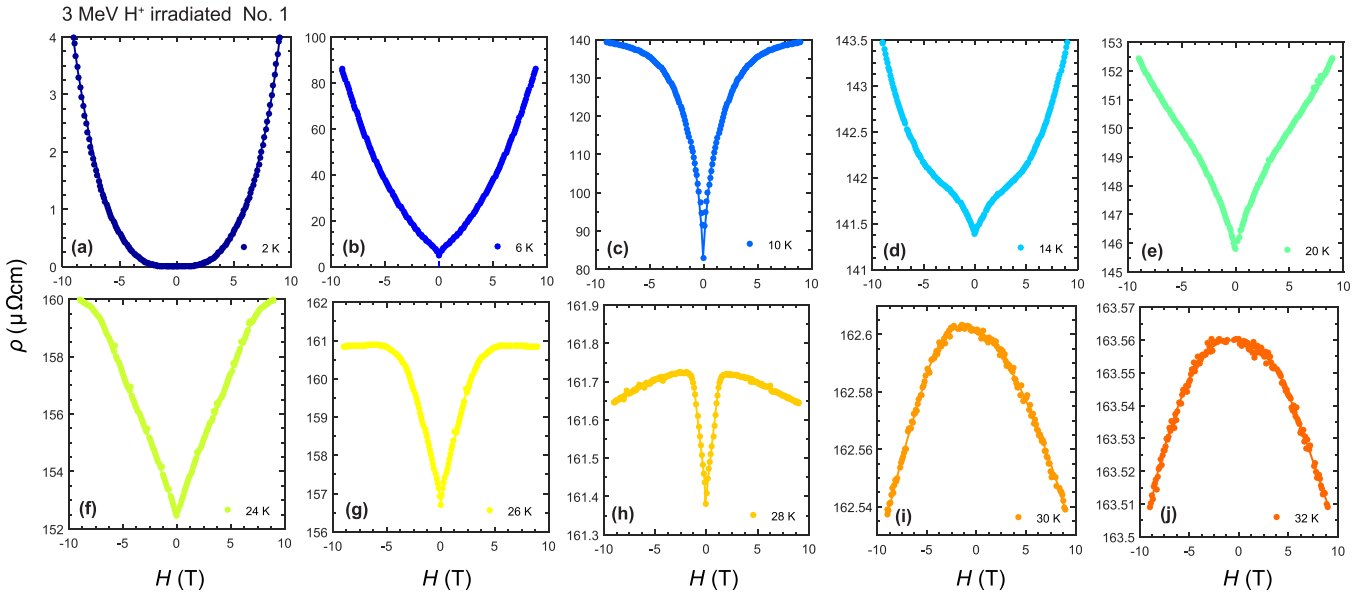

FIG. 9. The magnetoresistance of irradiated $BaFe_2(As_{0.67}P_{0.33})_2$ No. 1 between −9 and 9 T at temperatures of (a) 2 K, (b) 6 K, (c) 10 K, (d) 14 K, (e) 20 K, (f) 24 K, (g) 26 K, (h) 28 K, (i) 30 K, and (j) 32 K.

shows a significantly higher degree of paramagnetic signal at lower temperatures. A dip seen at temperatures below 30 K in the pristine sample owing to vortex expulsion is absent in the irradiated sample. The increase in magnetization at lower temperatures in the pristine sample represents the paramagnetism from the $BaFe_2As_2$ parent compound [41–43]. Yet the paramagnetic signal in the irradiated signal is significantly greater than that of the pristine one.

Concerning the irradiated sample, the monotonic increase in magnetization at low temperatures signifies the existence of paramagnetism, well described by Curie's law $\chi = C/T$, where C is the Curie constant. Fitting through a least-mean-squares method reveals that $C = 5.5 \times 10^{-2}$ emu^{-1} K^{-1} mol for the irradiated sample. Thus, the effective magnetic moment is estimated to be $\mu_{\text{eff}} = 0.662\mu_{\text{B}}$ per formula unit, obtained from the equation,

$$\mu_{\text{eff}} = \sqrt{(3k_{\text{B}}C)/N_{\text{A}}}. \tag{4}$$

The effective spin-only magnetic moments of local magnetic Fe ions with valencies of Fe^{3+} ($^6S_{1/2}$) and Fe^{2+} ($^5D_4$) free ions are given by

$$\mu_{\text{s}} = g\sqrt{S(S+1)}\mu_{\text{B}}, \tag{5}$$

in which $g = 2.0$ is the Landé g factor for electrons and $S = 5/2$ and 2 are the spin angular momenta for valencies Fe^{3+} and Fe^{2+} in the respective order [44]. This yields the effective magnetic moment of a single magnetic impurity $\mu_{\text{s}}(Fe^{3+}) = 5.9\mu_{\text{B}}$ and $\mu_{\text{s}}(Fe^{2+}) = 4.9\mu_{\text{B}}$. For simplification, we assume that the number of magnetic impurities emanating from the two possible valencies are equally existing hence, $\mu_{\text{s}} \approx 5.4\mu_{\text{B}}$, the average between the two. This allows for a crude estimation of the concentration of magnetic impurities $n_{\text{imp}} \approx \mu_{\text{eff}}/(2 \times 5.4\mu_{\text{B}})$ in which the factor of 1/2 accounts for the two Fe's in a single formula unit. Consequently, n_{imp} is approximately 6.1×10^{-2}/formula unit, an order smaller than the concentration of the dopant atom 6.6×10^{-1}/formula unit, suggesting a dilute, yet, definite effect of magnetic scattering in the participation of pair breaking after irradiation.

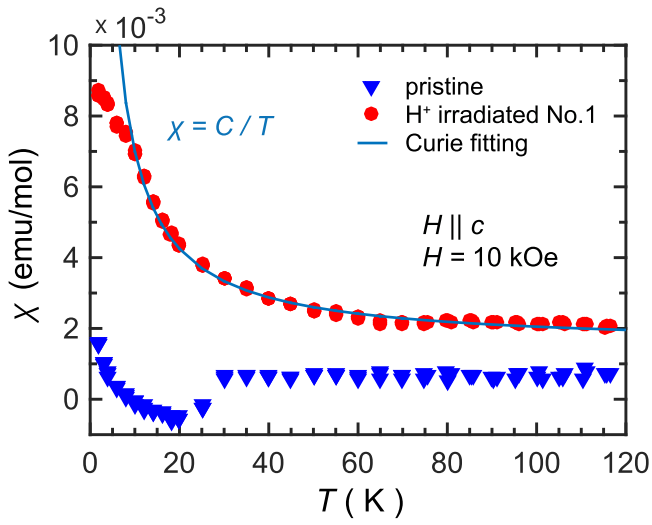

FIG. 10. The temperature dependence of magnetization of the H^+-irradiated and pristine sample No. 1 in a field of 10 kOe. The magnetization of the irradiated sample is fitted with Curie's law. The background of the sample holder is subtracted to ensure that the signal measured is entirely from the sample.

IV. DISCUSSIONS

It must be emphasized that the step feature below T_{c0} discussed previously and the negative magnetoresistance are two separate phenomena with different origins. The step feature occurs under the circumstance that there is coexistence of the superconducting and the normal phases on a macroscopic scale due to the magnified effect of irradiation under the terminal wires. However, at temperatures above

T_{c0} (e.g., 30 and 32 K) where superconductivity and the normal state cannot coexist, there is the appearance of negative magnetoresistance. The negative magnetoresistance together with magnetization data provide firm evidence of the presence of magnetic-scattering centers independent of the macroscopic inhomogeneities shown in Fig. 2.

The presence of local magnetic moments entails that the T_c reduction is an outcome of the formation of midgap states emanating from both magnetic and nonmagnetic scatterings. The slow suppression of T_c even in the presence of magnetic scattering produced by H^+ irradiation therefore, cannot completely rule out the s_{++}-gap symmetry scenario. However, it should be noted that the presence of magnetic impurities could be specific to the present system of $BaFe_2(As_{0.67}P_{0.33})_2$ since a negative MR is observed only in this system.

The whole scheme of differentiating a sign-changing or a sign-preserving superconducting gap in an iron-based superconductor is highly dependent on the assumption that the midgap states are generated solely through nonmagnetic scattering. Most reports concerning the effects of irradiation have assumed that the defects induced by irradiation are nonmagnetic due to the lack of temperature dependence representing Kondo scattering [18]. However, concerning optimal P-doped $BaFe_2As_2$, we see that, despite the lack of the logarithmic temperature-dependence characteristic of Kondo scattering, negative magnetoresistance and magnetization measurements have strongly indicated non-negligible incorporation of magnetic-scattering centers through irradiation. Although our investigation is limited to $BaFe_2(As_{0.67}P_{0.33})_2$, the possible generation of magnetic impurities could be present in other systems as well.

V. CONCLUSION

To sum up, throughout this paper, we have presented *in situ* resistivity measurements, STEM observation, magneto-transport measurements, and magnetization measurements of 3 MeV H^+-irradiated $BaFe_2(As_{0.67}P_{0.33})_2$ crystals. We have succeeded in suppressing T_c continuously down to zero. The observed suppression of T_c was slower than that of electron irradiation but faster than that of a He^+ particle. Such a trend holds for a wide range of different types of IBSs, implying that the defect morphology rather than the superconducting order parameter is the dominant influence for T_c suppression due to multiband physics.

After the irradiation, the B-linear resistivity of the sample, characteristic of the quantum critical state, collapses and is replaced by an anomalous negative MR. We discuss that the negative MR is most likely to emanate from sparse magnetic impurities. The presence of a paramagnetic signal recognized from magnetization measurements is a strong indication of the presence of magnetic impurities. Yet, the small effective magnetic moment suggests that the concentration of such magnetic impurities is dilute. This has also been exhibited by the lack of a Kondo-type logarithmic upturn, implying that most scatterers are still nonmagnetic. Yet, the contribution of magnetic scattering cannot simply be neglected.

ACKNOWLEDGMENTS

We would like to express our gratitude to T. Taen for fruitful discussions. This work was partly supported by KAKENHI (Grant No. 17H01141) from JSPS.

[1] P. W. Anderson, J. Phys. Chem. Solids **11**, 26 (1959).
[2] A. A. Abrikosov and L. P. Gor'kov, Sov. Phys. JETP **12**, 1243 (1961).
[3] V. Mishra, G. R. Boyd, S. Graser, T. Maier, P. J. Hirschfeld, and D. J. Scalapino, Phys. Rev. B **79**, 094512 (2009).
[4] A. A. Golubov and I. I. Mazin, Phys. Rev. B **55**, 15146 (1997).
[5] J. Li, Y. F. Guo, S. B. Zhang, J. Yuan, Y. Tsujimoto, X. Wang, C. I. Sathish, Y. Sun, S. Yu, W. Yi, K. Yamaura, E. Takayama-Muromachiu, Y. Shirako, M. Akaogi, and H. Kontani, Phys. Rev. B **85**, 214509 (2012).
[6] F. Han, X. Zhu, P. Cheng, G. Mu, Y. Jia, L. Fang, Y. Wang, H. Luo, B. Zeng, B. Shen, L. Shan, C. Ren, and H.-H. Wen, Phys. Rev. B **80**, 024506 (2009).
[7] Y. Nakajima, T. Taen, Y. Tsuchiya, T. Tamegai, H. Kitamura, and T. Murakami, Phys. Rev. B **82**, 220504 (2010).
[8] T. Taen, F. Ohtake, H. Akiyama, H. Inoue, Y. Sun, S. Pyon, T. Tamegai, and H. Kitamura, Phys. Rev. B **88**, 224514 (2013).
[9] S. Onari and H. Kontani, Phys. Rev. Lett. **103**, 177001 (2009).
[10] H. Kontani and S. Onari, Phys. Rev. Lett. **104**, 157001 (2010).
[11] Y. Wang, A. Kreisel, P. J. Hirschfeld, and V. Mishra, Phys. Rev. B **87**, 094504 (2013).
[12] R. Prozorov, M. Kończykowski, M. A. Tanatar, A. Thaler, S. L. Bud'ko, P. C. Canfield, V. Mishra, and P. J. Hirschfeld, Phys. Rev. X **4**, 041032 (2014).
[13] S. Kasahara, T. Shibauchi, K. Hashimoto, K. Ikada, S. Tonegawa, R. Okazaki, H. Shishido, H. Ikeda, H. Takeya, K. Hirata, T. Terashima, and Y. Matsuda, Phys. Rev. B **81**, 184519 (2010).
[14] J. M. Allred, K. M. Taddei, D. E. Bugaris, S. Avci, D. Y. Chung, H. Claus, C. dela Cruz, M. G. Kanatzidis, S. Rosenkranz, R. Osborn, and O. Chmaissem, Phys. Rev. B **90**, 104513 (2014).
[15] D. Hu, X. Lu, W. Zhang, H. Luo, S. Li, P. Wang, G. Chen, F. Han, S. R. Banjara, A. Sapkota, A. Kreyssig, A. I. Goldman, Z. Yamani, C. Niedermayer, M. Skoulatos, R. Georgii, T. Keller, P. Wang, W. Yu, and P. Dai, Phys. Rev. Lett. **114**, 157002 (2015).
[16] I. M. Hayes, R. D. McDonald, N. P. Breznay, T. Helm, P. J. W. Moll, M. Wartenbe, A. Shekhter, and J. G. Analytis, Nat. Phys. **12**, 916 (2016).
[17] M. Nakajima, S.-i. Uchida, K. Kihou, C.-H. Lee, A. Iyo, and H. Eisaki, J. Phys. Soc. Jpn. **81**, 104710 (2012).
[18] Y. Mizukami, M. Konczykowski, Y. Kawamoto, S. Kurata, S. Kasahara, K. Hashimoto, V. Mishra, A. Kreisel, Y. Wang, P. J. Hirschfeld, Y. Matsuda, and T. Shibauchi, Nat. Commun. **5**, 5657 (2014).
[19] M. P. Smylie, M. Leroux, V. Mishra, L. Fang, K. M. Taddei, O. Chmaissem, H. Claus, A. Kayani, A. Snezhko, U. Welp, and W.-K. Kwok, Phys. Rev. B **93**, 115119 (2016).
[20] C. Tarantini, M. Putti, A. Gurevich, Y. Shen, R. K. Singh, J. M. Rowell, N. Newman, D. C. Larbalestier, P. Cheng, Y. Jia, and H.-H. Wen, Phys. Rev. Lett. **104**, 087002 (2010).

[21] A. E. Karkin, J. Werner, G. Behr, and B. N. Goshchitskii, Phys. Rev. B **80**, 174512 (2009).
[22] K. Hashimoto, K. Cho, T. Shibauchi, S. Kasahara, Y. Mizukami, R. Katsumata, Y. Tsuruhara, T. Terashima, H. Ikeda, M. A. Tanatar, H. Kitano, N. Salovich, R. W. Giannetta, P. Walmsley, A. Carrington, R. Prozorov, and Y. Matsuda, Science **336**, 1554 (2012).
[23] C. J. van der Beek, M. Konczykowski, S. Kasahara, T. Terashima, R. Okazaki, T. Shibauchi, and Y. Matsuda, Phys. Rev. Lett. **105**, 267002 (2010).
[24] Y. Bang and G. R. Stewart, J. Phys.: Condens. Matter **29**, 123003 (2017).
[25] Y. Nakajima, Y. Tsuchiya, T. Taen, T. Tamegai, S. Okayasu, and M. Sasase, Phys. Rev. B **80**, 012510 (2009).
[26] T. Tamegai, T. Taen, H. Yagyuda, Y. Tsuchiya, S. Mohan, T. Taniguchi, Y. Nakajima, S. Okayasu, M. Sasase, H. Kitamura, T. Murakami, T. Kambara, and Y. Kanai, Supercond. Sci. Technol. **25**, 084008 (2012).
[27] T. Ozaki, L. Wu, C. Zhang, J. Jaroszynski, W. Si, J. Zhou, Y. Zhu, and Q. Li, Nat. Commun. **7**, 13036 (2016).
[28] J. F. Ziegler, M. D. Ziegler, and J. P. Biersack, Nucl. Instrum. Methods Phys. Res, Sect. B **268**, 1818 (2010).
[29] G. Blatter, M. V. Feigel'man, V. B. Geshkenbein, A. I. Larkin, and V. M. Vinokur, Rev. Mod. Phys. **66**, 1125 (1994).
[30] A. Pippard, *Magnetoresistance in Metals*, Cambridge Studies in Low Temperature Physics (Cambridge University Press, Cambridge, U.K., 1989) .
[31] A. E. Koshelev, Phys. Rev. B **88**, 060412 (2013).
[32] J. G. Analytis, H.-H. Kuo, R. D. McDonald, M. Wartenbe, P. M. C. Rourke, N. E. Hussey, and I. R. Fisher, Nat. Phys. **10**, 194 (2014).
[33] V. F. Gantmakher, M. V. Golubkov, J. G. S. Lok, and A. K. Geim, J. Exp. Theor. Phys. **82**, 951 (1996).
[34] *Hopping Transport in Solids*, edited by M. Pollak and B. I. Shklovskii, Modern Problems in Condensed Matter Sciences Vol. 28 (Elsevier, Amsterdam, 1991).
[35] Y. Dubi, Y. Meir, and Y. Avishai, Phys. Rev. B **73**, 054509 (2006).
[36] Y. Dubi, Y. Meir, and Y. Avishai, Nature (London) **449**, 876 (2007).
[37] H. Gretarsson, A. Lupascu, J. Kim, D. Casa, T. Gog, W. Wu, S. R. Julian, Z. J. Xu, J. S. Wen, G. D. Gu, R. H. Yuan, Z. G. Chen, N.-L. Wang, S. Khim, K. H. Kim, M. Ishikado, I. Jarrige, S. Shamoto, J.-H. Chu, I. R. Fisher, and Y.-J. Kim, Phys. Rev. B **84**, 100509 (2011).
[38] T. Van Peski-Tinbergen and A. J. Dekker, Physica **29**, 917 (1963).
[39] I. S. Blokhin, S. Y. Gavrilkin, B. P. Gorshunov, V. A. Dravin, E. S. Zhukova, O. M. Ivanenko, K. Iida, S. I. Krasnosvobodtsev, F. Kurth, K. V. Mitsen, and A. Y. Tsvetkov, JETP Lett. **101**, 247 (2015).
[40] M. Rotter, C. Hieke, and D. Johrendt, Phys. Rev. B **82**, 014513 (2010).
[41] S. Avci, O. Chmaissem, D. Y. Chung, S. Rosenkranz, E. A. Goremychkin, J. P. Castellan, I. S. Todorov, J. A. Schlueter, H. Claus, A. Daoud-Aladine, D. D. Khalyavin, M. G. Kanatzidis, and R. Osborn, Phys. Rev. B **85**, 184507 (2012).
[42] Y. Nakai, T. Iye, S. Kitagawa, K. Ishida, H. Ikeda, S. Kasahara, H. Shishido, T. Shibauchi, Y. Matsuda, and T. Terashima, Phys. Rev. Lett. **105**, 107003 (2010).
[43] S. Aswartham, M. Abdel-Hafiez, D. Bombor, M. Kumar, A. U. B. Wolter, C. Hess, D. V. Evtushinsky, V. B. Zabolotnyy, A. A. Kordyuk, T. K. Kim, S. V. Borisenko, G. Behr, B. Büchner, and S. Wurmehl, Phys. Rev. B **85**, 224520 (2012).
[44] A. Earnshaw, *Introduction to Magnetochemistry* (Academic, London, 1968) .